Journal of Molecular Graphics and Modelling 61 (2015) 53–60

Contents lists available at ScienceDirect

Journal of Molecular Graphics and Modelling

journal homepage: www.elsevier.com/locate/JMGM

Effects of imidazolium-based ionic liquids on the stability and dynamics of gramicidin A and lipid bilayers at different salt concentrations

Hwankyu Lee[a,*], Sun Min Kim[b], Tae-Joon Jeon[c]

[a] Department of Chemical Engineering, Dankook University, Yongin 448-701, South Korea
[b] Department of Mechanical Engineering, Inha University, Incheon 402-751, South Korea
[c] Department of Biological Engineering, Inha University, Incheon 402-751, South Korea

ARTICLE INFO

Article history:
Received 14 March 2015
Received in revised form 19 May 2015
Accepted 29 June 2015
Available online 2 July 2015

Keywords:
Ionic liquid
Gramicidin A
MD simulation
Lipid bilayer

ABSTRACT

Gramicidin A (gA) dimers with bilayers, which consist of phospholipids and ionic liquids (ILs) at different molar ratios, were simulated at different salt concentrations of 0.15 and 1 M NaCl. Bilayer thickness is larger than the length of a gA dimer, and hence lipids around the gA dimer are significantly disordered to adapt to the gA dimer, yielding membrane curvature. As the IL concentration increases, the bilayer thickness decreases and becomes closer to the gA length, leading to less membrane curvature. Also, ILs significantly increase lateral diffusivities of the gA dimer and lipids at 0.15 M NaCl, but not at 1 M NaCl because strong electrostatic interactions between salt ions and lipid head groups suppress an increase in the lateral mobility of the bilayer at high salt concentration. These findings help explain the conflicting experimental results that showed the increased ion permeability in electrophysiological experiments at 1 M NaCl, but the reduced ion permeability in fluorescent experiments at 0.15 M NaCl. ILs disorder lipids and make bilayers thinner, which yields less membrane curvature around the gA dimer and thus stabilizes the gA dimer, leading to the increased ion permeability. This IL effect predominantly occurs at 1 M NaCl, where ILs only slightly increase the bilayer dynamics because of the strong electrostatic interactions between salt ions and lipids. In contrast, at 0.15 M NaCl, ILs do not only stabilize the curved bilayer but also significantly increase the lateral mobility of gA dimers and lipids, which can reduce gA-induced pore formation, leading to the decreased ion permeability.

1. Introduction

Ionic liquids (ILs), which are large organic or inorganic ions in liquid phase at room temperature, have been considered to be good candidate solvents for use as electrolytes and sorption media for catalysis [1,2], battery [3,4], separation process [5,6], synthesis of composite materials [7,8], and hydrolysis of cellulose [9] because of their low volatility, non-flammability, high conductivity, and thermal and chemical stability [10–14]. Also, these thermal and chemical properties can be easily controlled by the combination of differently sized anions and cations [15]. However, experiments have shown that ILs are toxic to natural organisms in aquatic environments, which limits the use of ILs for many industrial and environmental applications [16–21]. To reduce cytotoxicity, the use of ILs at the low concentration has been suggested, while ILs still accumulate even at low concentrations because of their low degradability. Although these experiments clearly showed the toxicity of ILs at the organism level, the mechanism for the cytotoxicity of ILs has not been understood at the molecular level. To design ILs that have low toxicity but still maintain their thermal and chemical stability, the interactions between ILs and cell membranes need to be understood nearly at the atomic scale.

Experimentally, Evans showed that imidazolium-based ILs with longer hydrocarbon chains more significantly destabilize liposome membranes or supported lipid bilayers, indicating that lipid bilayers are disordered by the hydrophobic interactions between ILs and lipids [22–24]. Jeong et al. performed colorimetric assay with the liposome membrane, showing that ILs with longer chains at higher concentrations more effectively penetrate into membranes and thus decrease the membrane stability [25]. This was also confirmed by observing the reduced transition temperature of membranes for ILs with longer tails at high concentrations. Ryu et al. recently performed electrophysiological and fluorescent experiments with the peptide gramicidin A (gA) in the bilayer consisting of ILs and phospholipids [26]. Since the gA peptides, which laterally diffuse along each leaflet of the bilayer, can dimerize to form the ion chan-

* Corresponding author.
E-mail address: leeh@dankook.ac.kr (H. Lee).

http://dx.doi.org/10.1016/j.jmgm.2015.06.016
1093-3263/

nel, the stability and dynamics of the bilayer can be predicted by analyzing the extent of the gA-induced pore formation. Both electrophysiological and fluorescent experiments showed that larger ILs at higher concentrations induce the decreased conductance, implying that larger ILs more easily insert into the bilayer and thus induce the stronger repulsive interaction between Na^+ ions and the bilayer surface. In particular, electrophysiological experiments, which were performed at 1 M NaCl, showed that ILs induce the longer dwell time of the gA dimer, indicating the increased ion permeability, while in fluorescent experiments with much less ions (0.14 M $NaNO_3$), the ion permeability decreases with increasing the size and concentration of ILs. These apparently conflicting experimental results might be resolved by considering separately the effects of ILs and the salt concentration. It is quite possible that the effect of ILs on membrane properties is controlled not by any single factor, but by a combination of the size and concentration of ILs, and salt concentration.

Molecular dynamics (MD) simulations have been able to explore the interactions between imidazolium-based ILs and bilayers. Ballone and coworkers simulated ILs in cholesterol and phospholipid bilayers, showing that ILs insert into the bilayer, while inorganic counterions mostly interact with the bilayer surface or dissolve in water [27,28]. Klahn and Zacharias calculated free energies for the insertion of ILs into lipid bilayers, showing that cholesterols influence membrane structure and the electric strength of the bilayer surface, which impedes insertion of ILs into the bilayer [29]. Recently, our group simulated the insertion of ILs into lipid bilayers, showing that ILs with a tail of two or four hydrocarbons insert and reversibly detach from the bilayer, while the inserted longer ILs cannot be reversibly detached [30], in quantitative agreement with experiments [31]. We also found that the binding and insertion of ILs into the bilayer are modulated by both hydrophobic and electrostatic interactions, depending on the tail length of ILs [30]. These simulations have shown the dependence of binding and insertion on the IL-tail length, lipid component, and salt concentration, but their effects on the membrane curvature and stability have not yet been systematically studied through computation.

In this work, we therefore perform MD simulations of the bilayers composed of the gA dimer, ILs, and phospholipids. gA dimers are simulated in bilayers with different molar ratios of phospholipids and ILs at salt concentrations of 0.15 and 1 M NaCl. The bilayer thickness and disorder around the gA are analyzed, which are rationalized by the effects of ILs on the bilayer curvature and lateral mobility, and the electrostatic interactions between NaCl ions and bilayer surfaces. We will show that these results help explain the conflicting experimental observations regarding the effects of ILs on the stability of the gA-induced pore and membrane at different salt concentrations.

2. Methods

All simulations and analyses were performed using the GROMACS4.5.5 simulation package [32–34] with the OPLS all-atom force field (FF) [35,36] and TIP4P water model. Fig. 1 shows structures of IL and peptide gA. Potential parameters for IL (1-decyl-3-methylimidazolium; DMIM) were directly taken from the OPLS ionic-liquid FF, which was previously developed by Sambasivarao and Acevedo,[37] showing the structural and thermodynamic properties of ionic liquids and their solvent effects on polymer conformation [37,38], in agreement with experiments and polymer theories. The structure and coordinates of the peptide gA (formyl-VGALA VVVWL WLWLW-ethanolamine) were downloaded from the Protein Data Bank (PDB code: 1JNO) [39]. For dioleoylglycerophosphocholine (DOPC) lipids, Tieleman et al. modified the Berger lipid FF to be compatibly used with the OPLS FF [40],

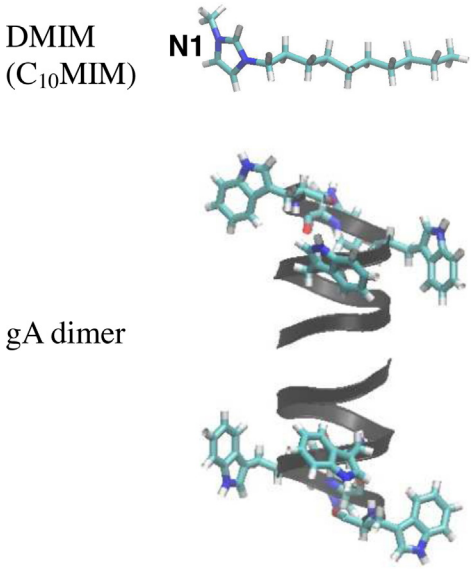

Fig. 1. Structures of an ionic liquid (DMIM; C_{10}MIM) and a gA dimer. Light-blue, red, blue, and white colors represent C, O, N, and H atoms, respectively. The N atom adjacent to the methyl group of DMIM is named "N1". For the gA dimer, the peptide backbone is represented as a black ribbon, and the side chain is shown only for tryptophan residues. The images were created with Visual Molecular Dynamics. [55].

which reproduces the experimentally observed areas per lipid and dynamics of DOPC bilayers [41].

Bilayer systems were generated with the mixture of DOPC and DMIM at four different molar ratios in periodic boxes of sizes 5.4–6.5 × 5.4–6.5 × 7.3–8.8 nm^3 (Table 1). The gA dimer, which forms an ion channel, was inserted into the bilayer center by using the protein-insertion tool (g_membed) implemented in the GROMACS package [42,43], and then several steps of energy minimization and an equilibration run of 500 ps were performed with position restraints applied to the peptide. The final system consists of a gA dimer, 122 DOPC or DMIM (61 DOPC or DMIM per leaflet), ~5000 water molecules, and enough Na^+ and Cl^- ions to neutralize the system, leading to the salt concentrations of 0.15 M and 1 M NaCl. Note that electrical and fluorescence experiments were performed at 1 M NaCl and 0.14 M $NaNO_3$, respectively [26]. In this work, salts of 1 M and 0.15 M NaCl were used to investigate the concentration effect of the same type of salt, although it cannot be ruled out that NaCl and $NaNO_3$ might yield different electrostatic properties of the simulated systems. Real space cutoffs of 14 Å and 11 Å were respectively applied for Lennard–Jones (LJ) and electrostatic forces with the inclusion of particle mesh Ewald summation [44] for long-range electrostatics. A temperature of 298 K, which is similar to the experimental condition [26], and a pressure of 1 bar were maintained by applying the velocity-rescale thermostat [45] and Berendsen barostat [46] in the $NP_{xy}P_zT$ ensemble (semi-isotropic pressure coupling). The LINCS algorithm was used to constrain the bond lengths.[47] Unrestrained equilibration runs were performed for 200 ns with a time step of 2 fs on computational facilities supported by the Supercomputing Center/Korea Institute of Science and Technology Information with supercomputing resources including technical support (KSC-2014-C3-68). The last-50 ns trajectories were used for analyses.

3. Results and discussion

Bilayers consisting of the gA dimer, DOPC lipids and DMIM ILs were simulated at different concentrations of ILs and NaCl ions. Table 1 lists the simulated systems. The first initials "GD" repre-

Table 1
List of simulations.

Name	Conc. of NaCl (M)	No. of molecules			Simulation time (ns)
		IL (DMIM)	DOPC	gA dimer	
GD0-0.15	0.15	–	122	1	200
GD0-1	1	–	122	1	200
GD13-0.15	0.15	16	106	1	200
GD13-1	1	16	106	1	200
GD26-0.15	0.15	31	90	1	200
GD26-1	1	31	90	1	200
GD52-0.15	0.15	63	58	1	200
GD52-1	1	63	58	1	200

sent the simulations for the "gA dimer" in the DOPC/DMIM bilayer, which are followed by the mol% of DMIMs in the bilayer. The last numbers "0.15" and "1" indicate the NaCl concentrations of 0.15 M and 1 M, respectively.

3.1. The effect of ionic liquids on the bilayer thickness

Fig. 2 shows final configurations for simulations of the gA dimer in the DOPC/DMIM bilayer. gA peptides show stable helical structure and dimeric conformation for whole simulation time. gA dimers are highly hydrophobic and thus interact with hydrocarbon tails of DOPC lipids and DMIMs. Note that thickness of the DOPC bilayer is larger than the z-dimensional size of the gA dimer, and hence the bilayer surface becomes curved to adapt to the smaller gA dimer, as visualized in Fig. 2. Fig. 3 shows the bilayer size in xy dimension as a function of time. Since DMIM (a single tail) is smaller than DOPC (two longer tails), the bilayer size decreases at the higher concentration of DMIM, as expected. The bilayer thickness was also calculated from the distance between average z values of phosphorus atoms for each leaflet. In Fig. 3, the bilayers at higher concentrations of DMIM become thinner, showing that DMIMs induce a decrease in the bilayer thickness, presumably because DMIMs disorder lipids. This is also confirmed by calculating the density and membrane-thickness profiles. In Fig. 4, density profiles show that the distance between phosphorus atoms of each leaflet is smaller in GD52-0.15 and GD52-1 than in other systems, consistent with Fig. 3. To obtain the bilayer-thickness profiles, the xy-plane parallel to the bilayer surface was equally divided into 121 voxels by using a grid (11×11 grid) [48]. For each voxel, the z components of DOPC's P atoms and DMIM's N1 atoms were averaged for each leaflet, and the difference in the z values between leaflets was taken to be the bilayer thickness. In Fig. 4 (bottom), the bilayer around the gA dimer is thinner (blue-colored region) than the bilayer far from the gA, again indicating that lipids are disordered to adapt to the smaller gA dimer. The region of thin bilayer becomes larger for the systems with more DMIMs, indicating that DMIMs reduce the bilayer thickness. Fig. 4 also shows that densities of N1 atoms of IL are overlapped with those of P atoms of DOPC, indicating the charge interactions between cationic IL headgroups and anionic DOPC phosphates. Tryptophan residues of the gA are close to the bilayer surface, implying their anchoring effect, as also observed from other simulations [49,50].

3.2. The effect of ionic liquids on the bilayer curvature and disorder around the gA dimer

As discussed above, the bilayers with more DMIMs become thinner and thus less curved around the gA dimer. To quantitatively analyze the extent of the bilayer curvature around the gA dimer, order parameters of DOPC tails were calculated from $S_{CC} = \frac{3}{2}(\cos^2\theta z) - \frac{1}{2}$, where θz is the angle that the vector connecting carbons C_{n-1}–C_{n+1} makes with the z-axis [51]. The bracket indicates averaging over time and over all molecules in the simulation. Order parameters can vary between 1 (perfect orientation in the interface normal direction) and $-1/2$ (perfect orientation perpendicular to the normal). Here, order parameters of DOPC tails were calculated within 1.3 nm of the center of mass (COM) of a gA dimer (xy dimension). Fig. 5 shows that order parameters of DOPC-tail carbons adjacent to the lipid head are higher for the systems with more DMIMs, indicating that lipids around the gA dimer are less disordered at higher concentrations of DMIM. This is because more DMIMs induce the thinner bilayer, where the bilayer thickness and the gA length become closer, and hence lipid tails adjacent to lipid heads do not have to be significantly disordered to adapt to the gA dimer, leading to less membrane curvature, as visualized in Figs. 2 and 5. Note that at higher concentrations of DMIM, order parameters of lipid tails close to the lipid head are higher, while those around the bilayer center (the tail end) are lower, which seem to conflict. This is presumably because tail ends around the bilayer center do not need to be disordered to adapt to the gA length, and hence their order parameters are predominantly influenced by the disorder effect of DMIMs, while lipid tails close to the lipid head are more significantly modulated by the gA-induced curvature than by the DMIM-induced disorder effect.

To confirm this, the solvent accessible surface areas (SASA) of gA dimers were calculated, which is defined to be the peptide area uncovered by DOPCs and ILs. Fig. 6 shows that the number of DMIMs around the gA increases as the concentration of DMIMs increases, showing that gA dimers interact with DOPCs as well as DMIMs, as expected. In particular, higher concentrations of DMIMs cause a decrease in the bilayer thickness as well as an increase in the SASA of gA dimers, indicating that the bilayer surface around the gA dimer is less curved in the thinner bilayer, and thus gA dimers are more exposed to water in the thinner bilayer than in the thicker bilayer, consistent with the observation in Fig. 5. These results imply that the higher concentration of DMIM can more effectively reduce membrane curvature around the gA dimer and thus possibly stabilize the gA-induced pore, leading to the increases in the dwell time of gA dimers and the ion permeability, which supports Ryu et al.'s electrophysiological experiments [26].

3.3. The effect of the salt concentration on the stability and dynamics of the bilayer

Although these simulation results support electrophysiological experiments that were performed at 1 M NaCl and showed that higher concentrations of ILs induce longer dwell times of gA dimers, they still conflict with fluorescent experiments at 0.15 M NaCl that showed that more ILs yield the lower rates of fluorescence quenching [26]. These indicate that ILs promote the pore formation of the gA dimer and thus induce the higher ion permeability in electrophysiological experiments, which conflicts with fluorescent experiments that showed less pore formation and ion permeability. These opposite observations might be induced by different salt con-

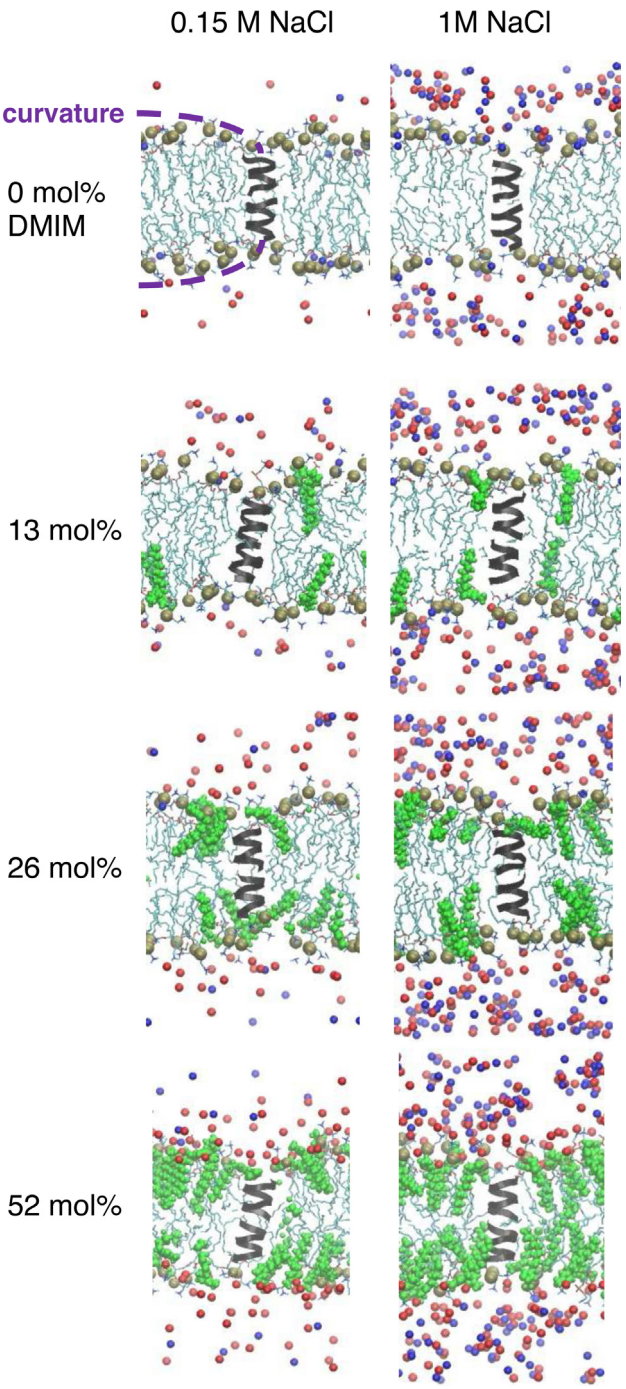

Fig. 2. Final snapshots of simulations of the gA dimer with DOPC/DMIM bilayers at different concentrations of DMIM and NaCl ions. Black (ribbons), green, brown, light blue, blue and red colors represent gA dimers, ILs (DMIM), DOPC phosphorus atoms, DOPC tails, Na^+ and Cl^- ions, respectively. Water molecules are omitted for clarity. (For interpretation of the references to color in this figures legend, the reader is referred to the web version of this article.)

ditions, which can influence the stability of gA-induced pores and membrane dynamics. To resolve this, lateral diffusion coefficients of DOPC lipids and gA dimers were calculated from the slopes of the mean-square displacements (MSD) in the xy-plane (the direction perpendicular to the bilayer normal). Note that simulations were performed with periodic boundary conditions, and thus the MSD needs to be corrected for finite size effects. This is analytically well formulated for simulations of cubic boxes [52], but not for those of noncubic boxes with bilayers. Also, the size effect should not significantly affect the comparison of lateral diffusivities, since the sizes of simulated systems do not significantly differ. Thus, the finite size effect is not corrected. In Fig. 7, as the DMIM concentration increases, lateral diffusivities of DOPC lipids become higher, again indicating that DMIMs disorder lipids and thus increase the bilayer dynamics. Lateral diffusivities are higher at 0.15 M NaCl than at 1 M NaCl, indicating the dependence on the NaCl concentration. In particular, diffusion coefficients drastically increase in the bilayers with DMIMs of 26 and 52 mol% at 0.15 M NaCl, while those values are even saturated and do not increase at 1 M NaCl. Lateral diffusivities of gA dimers show the same trend with relatively lower values, apparently because of the larger size of gA dimers. These indicate that DMIMs disorder DOPC lipids and thus increase their lateral mobility at 0.15 M NaCl, but this increase in lateral diffusivity can be impeded at the higher concentration of 1 M NaCl, implying that the salt concentration modulates the effects of ILs on the bilayer dynamics.

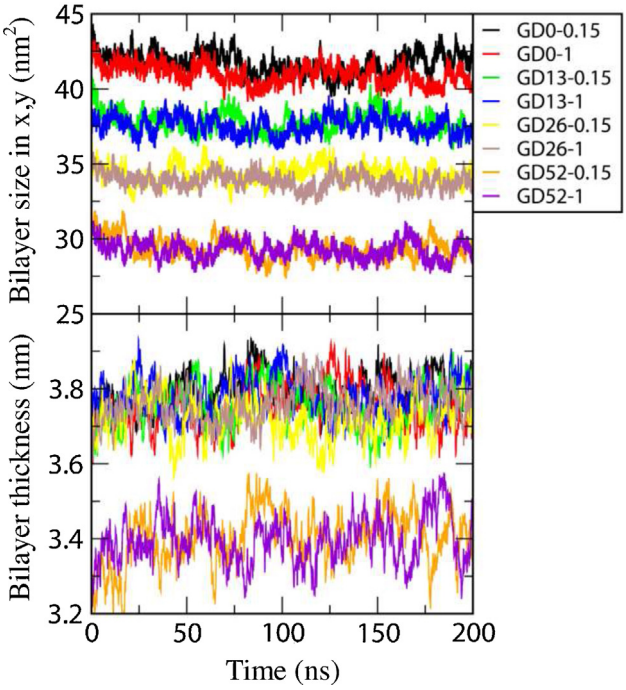

Fig. 3. The bilayer size in xy dimension (top) and the bilayer thickness (bottom) as functions of time.

To understand the interactions between the bilayer and Na^+ ions, we calculated radial distribution functions (RDFs) between Na^+ ions and phosphorous atoms of anionic DOPC phosphates. In Fig. 8, the systems with more DMIMs show lower peaks at both 0.15 and 1 M NaCl, indicating that Na^+ ions are less concentrated around the bilayer surface because of the electrostatic repulsion between cationic DMIMs and Na^+ ions, in agreement with experimental observations of a decreased conductance at higher concentrations of DMIMs [26]. Although RDF peaks become lower at both 0.15 and 1 M NaCl, the extent of decreasing is larger at 0.15 M than at 1 M, indicating that ILs inhibit the electrostatic binding of Na^+ ions into DOPC phosphates more significantly at 0.15 M NaCl than at 1 M, consistent with the trend of lateral diffusivities in Fig. 7. Also, note that, regardless of the DMIM concentration, RDF peaks are much higher at 1 M NaCl than at 0.15 M. This indicates the stronger interactions between Na^+ ions and lipid head groups at 1 M, which can inhibit an increase in the lateral mobility of bilayers, as previously observed in experiments and simulations [53,54].

In addition to this effect of Na^+ ions, Cl^- ions might also influence the bilayer mobility. Note that previous simulations have shown

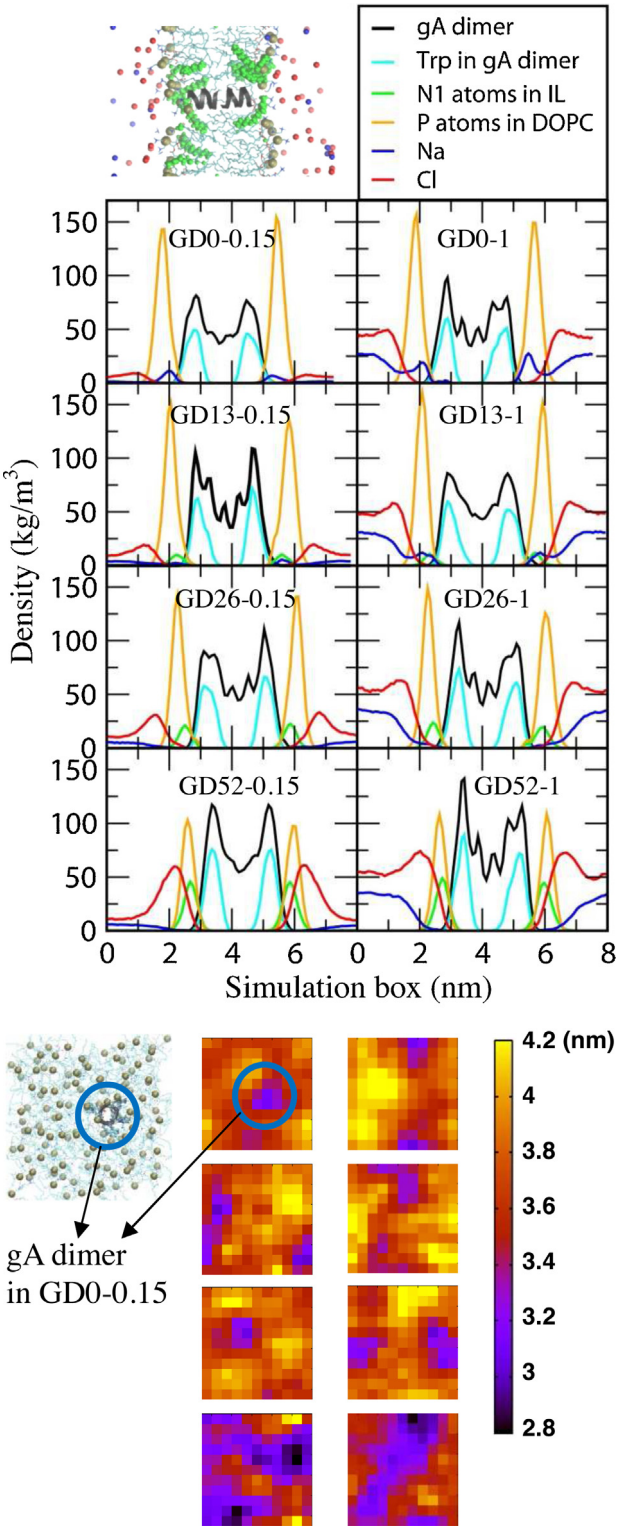

Fig. 4. (a) Mass density (top, averaged over the last 50 ns) and (b) bilayer thickness profiles (bottom, 200 ns). The bilayer-thickness profiles are represented with different colors, which were created with GridMAT-MD [48], and arranged in the same order of the mass-density profiles.

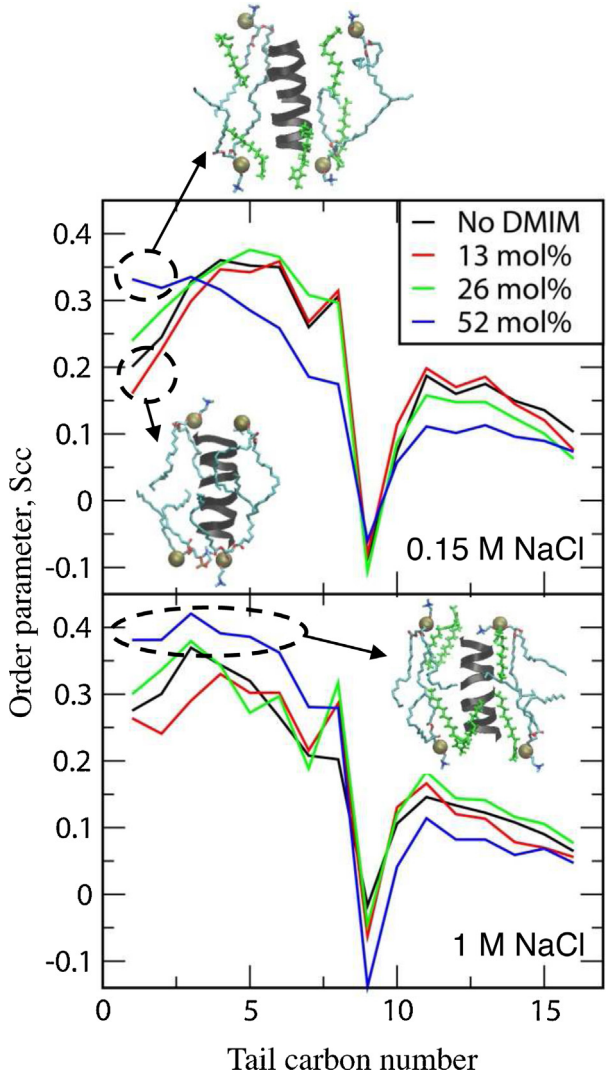

Fig. 5. Order parameters of DOPC tails within a distance (xy dimension) of 1.3 nm of the COM of the gA dimer.

that Cl^- ions do not directly bind to the bilayer surface, but those in the aqueous phase modulate the orientation of lipid headgroups. To examine the effect of Cl^- ions, the orientations of lipid headgroups were determined by calculating the tilt angle, which we define as the angle between the bilayer normal and the vector connecting P and N atoms of the DOPC headgroup. Fig. 9 shows that average tilt angles do not differ at 0.15 and 1 M NaCl regardless of the DMIM concentration, indicating no effect of the NaCl concentration within this range. Interestingly, tilt angles drastically decrease as the DMIM concentration increases, presumably because lipid headgroups have to be tilted to adapt to the gA length at lower concentrations of DMIM, but not in the thinner bilayer at higher concentrations of DMIM, consistent with our above-mentioned results. In Fig. 9 (bottom), RDFs between phosphorus atoms of lipids show no difference at 0.15 and 1 M NaCl, which indicates that salt ions do not directly influence bilayer properties, although their lateral diffusivities significantly differ (Fig. 7). These results indicate that the slower mobility of bilayers is attributed entirely to the strong charge interactions between Na^+ ions and lipid head groups.

These simulation findings help explain the conflicting experimental observations regarding the effects of ILs on the ion permeability of gA-induced pores in electrophysiological and fluorescent experiments. For the bilayers without ILs, DOPC lipids need to be disordered to adapt to the smaller gA dimer, which induces membrane curvature around the gA. However, as the concentration of ILs increases, ILs disorder lipids and make the bilayer thinner, and thus the bilayer thickness and the length of the gA dimer become closer, leading to the less bilayer curvature around

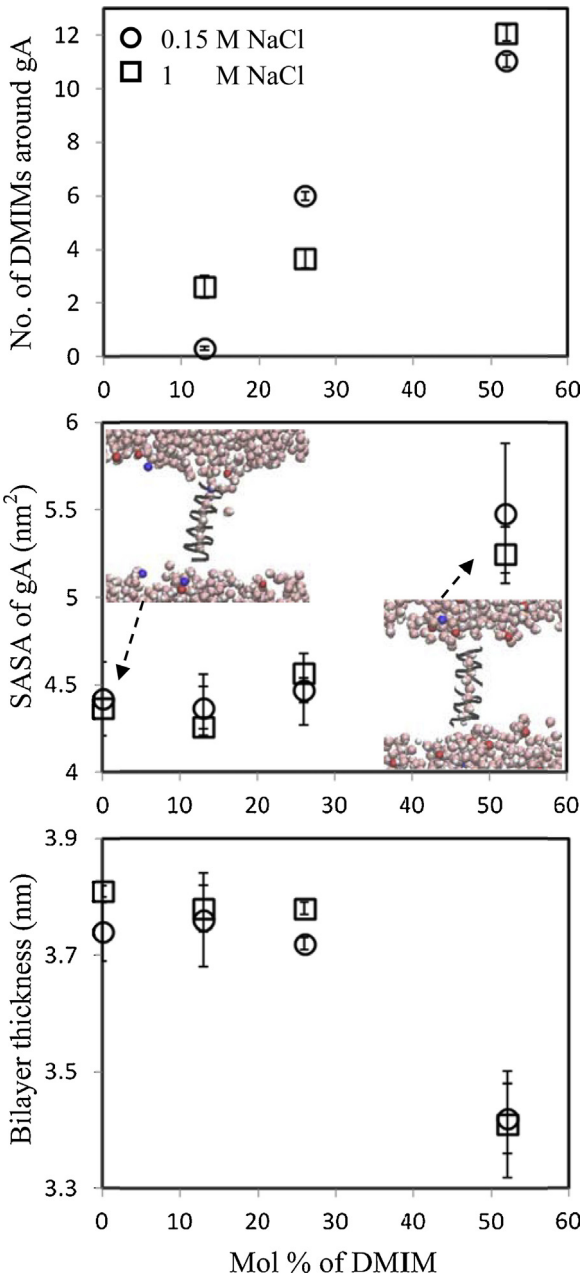

Fig. 6. The numbers of DMIMs around a gA dimer (top), solvent accessible surface areas (SASA) of a gA dimer (middle), and thickness of the bilayer (bottom) as a function of the DMIM concentration. In the snapshots at DMIM concentrations of 0 and 52 mol%, DOPC lipids and DMIMs are omitted to clearly visualize the curvature of the bilayer surface around the gA.

the gA, which can possibly increase the stability of the gA dimer. Since gA dimers can be stabilized by ILs, their dwell times also increase, leading to the increased ion permeability. Besides this IL effect, since ILs disorder lipids, they can also increase the lateral mobility of lipids and gA peptides, which may induce less stable gA dimers and pore formation, leading to the decreased ion permeability. These opposite effects can be predominant at either low or high salt concentrations. Since electrophysiological experiments were performed at 1 M NaCl, the effects of ILs on the interaction between Na^+ and the bilayer surface become weaker, and hence the attractive electrostatic interactions between lipid head groups and Na^+ ions suppress the lateral translation of the gA and lipids, which allows ILs to predominantly stabilize the bilayer around the gA dimer and increase the stability of gA-induced pores and ion

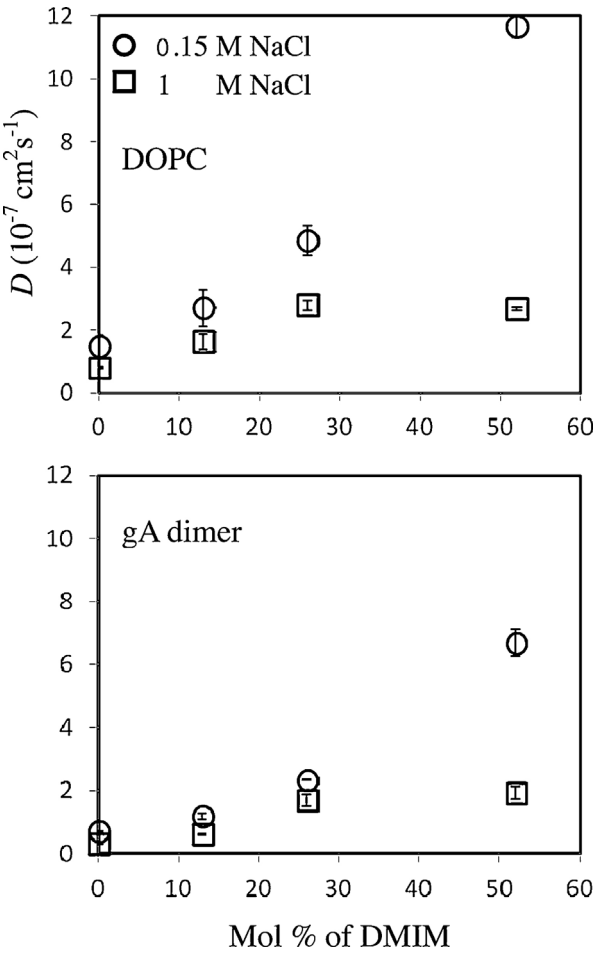

Fig. 7. Lateral diffusion coefficients (D) of DOPC lipids (top) and gA dimers (bottom) at the NaCl concentrations of 0.15 (○) and 1 M (□), as a function of the molar ratio of DMIM in the bilayer.

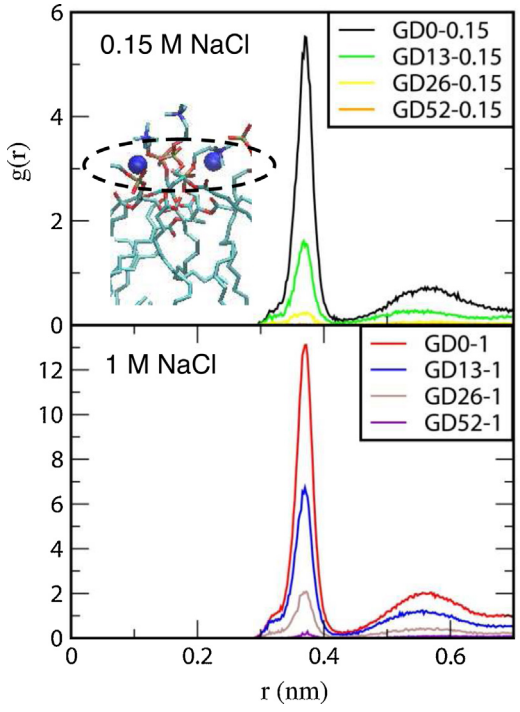

Fig. 8. Radial distribution functions between Na^+ ions and P atoms of DOPC phosphates at the concentrations of 0.15 and 1 M NaCl.

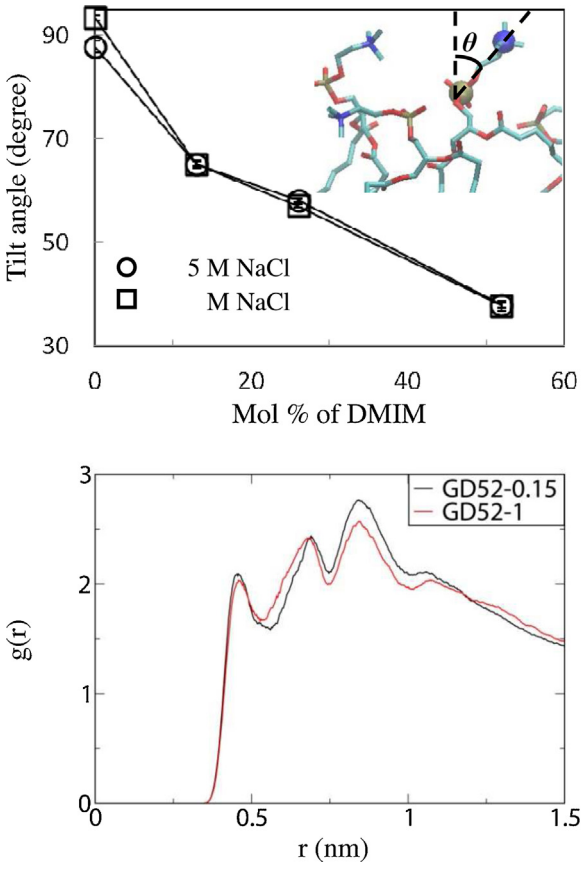

Fig. 9. Average tilt angles of DOPC headgroups, computed by calculating the angle between the P-N vector and the bilayer normal (z axis), with 0° representing a vertical orientation and 90° a horizontal one (top image), and radial distribution functions between P atoms of DOPC lipids (bottom image).

permeability. In the fluorescent experiments at 0.15 M NaCl, ILs do not only stabilize the curved bilayer around the gA dimer but also significantly increase lateral diffusivities of gA peptides and lipids, which possibly reduces the dwell time of the gA dimer, leading to the reduced ion permeability. These indicate that the effects of ILs on the stability and dynamics of lipid bilayers can be modulated by the salt concentration, which can help in the rational design of synthetic ILs with low toxicity for industrial and environmental applications.

4. Conclusions

To understand the conflicting experimental observations regarding the effect of ILs on the ion permeability through gA dimers in lipid bilayers, we performed MD simulations of gA dimers with lipid bilayers consisting of DOPC lipids and DMIM ILs at different molar ratios. Lipids are disordered to adapt to the smaller gA dimer, and hence the bilayer surface is curved around the gA dimer. As the concentration of DMIMs increases, the bilayer thickness decreases and becomes closer to the length of the gA dimer, and thus bilayer surfaces are less curved to adapt to the gA dimer. Lateral diffusion coefficients of gA dimers and lipids were calculated, which show the higher diffusivities for the bilayers with more DMIMs, indicating that DMIMs disorder lipids. In particular, lateral diffusivities drastically increase with increasing DMIMs at 0.15 M NaCl, while lateral diffusivities only slightly increase at 1 M NaCl because the stronger electrostatic interactions between Na^+ ions and DOPC phosphates inhibit an increase in the bilayer dynamics. These simulation findings may explain the conflicting experimental results that showed that ILs induce the higher ion permeability through the gA dimer in electrophysiological experiments at 1 M NaCl, but the lower ion permeability in fluorescence experiments at 0.15 M NaCl. ILs disorder lipids and induce the thinner bilayer, and hence the bilayer surface becomes less curved around the gA dimer, which can possibly increase the bilayer stability and dwell time of the gA, leading to the increased ion permeability. At 1 M NaCl, this effect predominantly occurs, since ILs only slightly increase the lateral dynamics of the bilayer because of the strong electrostatic interactions between ions and lipid head groups. However, at 0.15 M NaCl, ILs disorder lipids and significantly increase the lateral dynamics of the gA and lipids, which becomes more predominant, leading to the decreased gA-induced pore formation and ion permeability.

Acknowledgments

The present research was conducted by the research fund of Dankook University in 2014.

References

[1] Z. Conrad Zhang, Catalysis in Ionic Liquids. In: Advances in Catalysis, 2006, Vol. 49, pp. 153–237.
[2] T. Welton, Ionic liquids in catalysis, Coord. Chem. Rev. 248 (2004) 2459–2477.
[3] H. Saruwatari, T. Kuboki, T. Kishi, S. Mikoshiba, N. Takami, Imidazolium ionic liquids containing LiBOB electrolyte for lithium battery, J. Power Sources 195 (2010) 1495–1499.
[4] T. Kuboki, T. Okuyama, T. Ohsaki, N. Takami, Lithium-air batteries using hydrophobic room temperature ionic liquid electrolyte, J. Power Sources 146 (2005) 766–769.
[5] X. Han, D.W. Armstrong, Ionic liquids in separations, Acc. Chem. Res. 40 (2007) 1079–1086.
[6] M. Smiglak, A. Metlen, R.D. Rogers, The second evolution of ionic liquids: from solvents and separations to advanced materials – Energetic examples from the ionic liquid cookbook, Acc. Chem. Res. 40 (2007) 1182–1192.
[7] T.P. Lodge, Materials science: a unique platform for materials design, Science 321 (2008) 50–51.
[8] Y. He, Z. Li, P. Simone, T.P. Lodge, Self-assembly of block copolymer micelles in an ionic liquid, J. Am. Chem. Soc. 128 (2006) 2745–2750.
[9] R. Rinaldi, R. Palkovits, F. Schüth, Depolymerization of cellulose using solid catalysts in ionic liquids, Angew. Chem. – Int. Ed. 47 (2008) 8047–8050.
[10] N.V. Plechkova, K.R. Seddon, Applications of ionic liquids in the chemical industry, Chem. Soc. Rev. 37 (2008) 123–150.
[11] P. Wasserscheid, Chemistry volatile times for ionic liquids, Nature 439 (2006) 797.
[12] M.J. Earle, J.M.S.S. Esperança, M.A. Gilea, J.N.C. Lopes, L.P.N. Rebelo, J.W. Magee, et al., The distillation and volatility of ionic liquids, Nature 439 (2006) 831–834.
[13] T. Ueki, M. Watanabe, Macromolecules in ionic liquids: progress, challenges, and opportunities, Macromolecules 41 (2008) 3739–3749.
[14] J.S. Wilkes, A short history of ionic liquids – from molten salts to neoteric solvents, Green Chem. 4 (2002) 73–80.
[15] Y. Pu, N. Jiang, A.J. Ragauskas, Ionic liquid as a green solvent for lignin, J. Wood Chem. Technol. 27 (2007) 23–33.
[16] A. Latała, P. Stepnowski, M. Nędzi, W. Mrozik, Marine toxicity assessment of imidazolium ionic liquids: acute effects on the Baltic algae *Oocystis* submarina and Cyclotella meneghiniana, Aquat. Toxicol. 73 (2005) 91–98.
[17] R.J. Bernot, M.A. Brueseke, M.A. Evans-White, G.A. Lamberti, Acute and chronic toxicity of imidazolium-based ionic liquids on *Daphnia magna*, Environ. Toxicol. Chem. 24 (2005) 87–92.
[18] J. Pernak, K. Sobaszkiewicz, I. Mirska, Anti-microbial activities of ionic liquids, Green Chem. 5 (2003) 52–56.
[19] C. Pretti, C. Chiappe, D. Pieraccini, M. Gregori, F. Abramo, G. Monni, et al., Acute toxicity of ionic liquids to the zebrafish (*Danio rerio*), Green Chem. 8 (2006) 238–240.
[20] R.P. Swatloski, J.D. Holbrey, R.D. Rogers, Ionic liquids are not always green: hydrolysis of 1-butyl- methylimidazolium hexafluorophosphate, Green Chem. 5 (2003) 361–363.
[21] M. Petkovic, K.R. Seddon, L.P.N. Rebelo, C. Silva Pereira, Ionic liquids: a pathway to environmental acceptability, Chem. Soc. Rev. 40 (2011) 1383–1403.
[22] K.O. Evans, Room-temperature ionic liquid cations act as short-chain surfactants and disintegrate a phospholipid bilayer. Colloids and Surfaces A: Physicochemical and Engineering Aspects. 2006, 274, 11–17.
[23] K.O. Evans, Supported phospholipid bilayer interaction with components found in typical room-temperature ionic liquids – a QCM-D and AFM study, Int. J. Mol. Sci. 9 (2008) 498–511.

[24] K.O. Evans, Supported phospholipid membrane interactions with 1-butyl-3-methylimidazolium chloride, J. Phys. Chem. B 112 (2008) 8558–8862.
[25] S. Jeong, S.H. Ha, S.H. Han, M.C. Lim, S.M. Kim, Y.R. Kim, et al., Elucidation of molecular interactions between lipid membranes and ionic liquids using model cell membranes, Soft Matter 8 (2012) 5501–5506.
[26] H. Ryu, H. Lee, S. Iwata, S. Choi, M.K. Kim, Y.R. Kim, et al., Investigation of Ion Channel Activities of Gramicidin A in the Presence of Ionic Liquids Using Model Cell Membranes. *Scientific Reports* (2015) In Press.
[27] S.R.T. Cromie, M.G. Del Pópolo, P. Ballone, Interaction of room temperature ionic liquid solutions with a cholesterol bilayer, J. Phys. Chem. B 113 (11) (2009) 642–11648.
[28] R.J. Bingham, P. Ballone, Computational study of room-temperature ionic liquids interacting with a POPC phospholipid bilayer, J. Phys. Chem. B 116 (11) (2012) 11205–11216.
[29] M. Klähn, M. Zacharias, Transformations in plasma membranes of cancerous cells and resulting consequences for cation insertion studied with molecular dynamics, Phys. Chem.Chem. Phys. 15 (2013) 14427–14441.
[30] H. Lee, T.J. Jeon, The binding and insertion of imidazolium-based ionic surfactants into lipid bilayers: the effects of surfactant size and salt concentration, Phys. Chem. Chem. Phys. 17 (2015) 5725–5733.
[31] M. Galluzzi, S. Zhang, S. Mohamadi, A. Vakurov, A. Podestà, A. Nelson, Interaction of imidazolium-based room-temperature ionic liquids with DOPC phospholipid monolayers: electrochemical study, Langmuir 29 (2013) 6573–6581.
[32] D. Van Der Spoel, E. Lindahl, B. Hess, G. Groenhof, A.E. Mark, H.J.C. Berendsen, GROMACS: fast, flexible, and free, J. Comput. Chem. 26 (2005) 1701–1718.
[33] E. Lindahl, B. Hess, D. van der Spoel, GROMACS 3.0: a package for molecular simulation and trajectory analysis, J. Mol. Model. 7 (2001) 306–317.
[34] B. Hess, C. Kutzner, D. van der Spoel, E. Lindahl, GROMACS 4: algorithms for highly efficient, load-balanced, and scalable molecular simulation, J. Chem. Theory Comput. 4 (2008) 435–447.
[35] G.A. Kaminski, R.A. Friesner, J. Tirado-Rives, W.L. Jorgensen, Evaluation and reparametrization of the OPLS-AA force field for proteins via comparison with accurate quantum chemical calculations on peptides, J. Phys. Chem. B 105 (2001) 6474–6487.
[36] W.L. Jorgensen, D.S. Maxwell, J. Tirado-Rives, Development and testing of the OPLS all-atom force field on conformational energetics and properties of organic liquids, J. Am. Chem. Soc. 118 (11) (1996) 225–236.
[37] S.V. Sambasivarao, O. Acevedo, Development of OPLS-AA force field parameters for 68 unique ionic liquids, J. Chem. Theory Comput. 5 (2009) 1038–1050.
[38] J. Mondal, E. Choi, A. Yethiraj, Atomistic simulations of poly (ethylene oxide) in water and an ionic liquid at room temperature, Macromolecules 47 (2014) 438–446.
[39] L.E. Townsley, W.A. Tucker, S. Sham, J.F. Hinton, Structures of gramicidins A–C incorporated into sodium dodecyl sulfate micelles, Biochemistry 40 (2001) 11676–11686.
[40] D.P. Tieleman, J.L. MacCallum, W.L. Ash, C. Kandt, Z. Xu, L. Monticelli, Membrane protein simulations with a united-atom lipid and all-atom protein model: lipid-protein interactions, side chain transfer free energies and model proteins, J. Phys. Condens. Matter 18 (2006) S1221–S1234.
[41] E. Han, H. Lee, Effect of the structural difference between Bax-α5 and Bcl-xL-α5 on their interactions with lipid bilayers, Phys. Chem. Chem. Phys. 16 (2014) 981–988.
[42] M.G. Wolf, M. Hoefling, C. Aponte-SantamaríA, H. Grubmüller, G. Groenhof G-membed, Efficient insertion of a membrane protein into an equilibrated lipid bilayer with minimal perturbation, J. Comput. Chem. 31 (2010) 2169–2174.
[43] B. Sommer, Membrane packing problems: a short review on computational membrane modeling methods and tools, Comput. Struct. Biotechnol. J. 5 (2013) e201302014.
[44] U. Essmann, L. Perera, M.L. Berkowitz, T. Darden, H. Lee, L.G. Pedersen, A smooth particle Mesh Ewald Method, J. Chem. Phys. 103 (1995) 8577–8593.
[45] G. Bussi, D. Donadio, M. Parrinello, Canonical sampling through velocity rescaling, J. Chem. Phys. 126 (2007) 014101.
[46] H.J.C. Berendsen, J.P.M. Postma, W.F. van Gunsteren, A. DiNola, J.R. Haak, Molecular-dynamics with coupling to an external bath, J. Chem. Phys. 81 (1984) 3684–3690.
[47] B. Hess, P-LINCS: a parallel linear constraint solver for molecular simulation, J. Chem.Theory Comput. 4 (2008) 116–122.
[48] W.J. Allen, J.A. Lemkul, D.R. Bevan, GridMAT-MD: A grid-based membrane analysis tool for use with molecular dynamics, J. Comput. Chem. 30 (2009) 1952–1958.
[49] T. Kim, K.I. Lee, P. Morris, R.W. Pastor, O.S. Andersen, W. Im, Influence of hydrophobic mismatch on structures and dynamics of gramicidin A and lipid bilayers, Biophys. J. 102 (2012) 1551–1560.
[50] J. Yoo, Q. Cui, Three-dimensional stress field around a membrane protein: atomistic and coarse-grained simulation analysis of gramicidin A, Biophys. J. 104 (2013) 117–127.
[51] E. Egberts, H.J.C. Berendsen, Molecular-dynamics simulation of a smectic liquid-crystal with atomic detail, J. Chem. Phys. 89 (1988) 3718–3732.
[52] I.C. Yeh, G. Hummer, System-size dependence of diffusion coefficients and viscosities from molecular dynamics simulations with periodic boundary conditions, J. Phys. Chem. B 108 (2004) 15873–15879.
[53] R.A. Böckmann, A. Hac, T. Heimburg, H. Grubmüller, Effect of sodium chloride on a lipid bilayer, Biophys. J. 85 (2003) 1647–1655.
[54] A.A. Gurtovenko, Asymmetry of lipid bilayers induced by monovalent salt: atomistic molecular-dynamics study, J. Chem. Phys. 122 (2005).
[55] W. Humphrey, A. Dalke, K. Schulten, VMD: visual molecular dynamics, J. Mol. Graphics 14 (1996) 33–38.